JACC: CARDIOVASCULAR IMAGING
VOL. ■, NO. ■, 2014

ISSN 1936-878X/$36.00
PUBLISHED BY ELSEVIER INC.
http://dx.doi.org/10.1016/j.jcmg.2014.08.003

Quantification of Myocardial Blood Flow in Absolute Terms Using ^{82}Rb PET Imaging

Results of RUBY-10 Study

Sergey V. Nesterov, MD, PhD, PMP,*† Emmanuel Deshayes, MD, MSc,‡§ Roberto Sciagrà, MD,‖ Leonardo Settimo, MD,‖ Jerome M. Declerck, PhD,¶ Xiao-Bo Pan, PhD,¶ Keiichiro Yoshinaga, MD, PhD,# Chietsugu Katoh, MD, PhD,# Piotr J. Slomka, PhD,** Guido Germano, PhD,** Chunlei Han, MD, PhD,* Ville Aalto, MSc,* Adam M. Alessio, PhD,†† Edward P. Ficaro, PhD,‡‡ Benjamin C. Lee, PhD,§§ Stephan G. Nekolla, PhD,‖‖ Kilem L. Gwet, PhD,¶¶ Robert A. deKemp, PhD, PEng, PPhys,## Ran Klein, PhD,## John Dickson, PhD,*** James A. Case, MD, PhD,††† Timothy Bateman, MD, PhD,††† John O. Prior, MD, PhD,‡ Juhani M. Knuuti, MD, PhD*

ABSTRACT

OBJECTIVES The purpose of this study was to compare myocardial blood flow (MBF) and myocardial flow reserve (MFR) estimates from rubidium-82 positron emission tomography (^{82}Rb PET) data using 10 software packages (SPs): Carimas, Corridor4DM, FlowQuant, HOQUTO, ImagenQ, MunichHeart, PMOD, QPET, syngo MBF, and UW-QPP.

BACKGROUND It is unknown how MBF and MFR values from existing SPs agree for ^{82}Rb PET.

METHODS Rest and stress ^{82}Rb PET scans of 48 patients with suspected or known coronary artery disease were analyzed in 10 centers. Each center used 1 of 10 SPs to analyze global and regional MBF using the different kinetic models implemented. Values were considered to agree if they simultaneously had an intraclass correlation coefficient $>$0.75 and a difference $<$20% of the median across all programs.

RESULTS The most common model evaluated was the 1-tissue compartment model (1TCM) by Lortie et al. in 2007. MBF values from 7 of 8 SPs implementing this model agreed best (Carimas, Corridor4DM, FlowQuant, PMOD, QPET, syngo MBF, and UW-QPP). Values from 2 other models (El Fakhri et al. in Corridor4DM and Alessio et al. in UW-QPP) also agreed well, with occasional differences. The MBF results from other models (Sitek et al. 1TCM in Corridor4DM, Katoh et al. 1TCM in HOQUTO, Herrero et al. 2-tissue compartment model in PMOD, Yoshida et al. retention in ImagenQ, and Lautamäki et al. retention in MunichHeart) were less in agreement with Lortie 1TCM values.

CONCLUSIONS SPs using the same kinetic model, as described in Lortie et al. in 2007, provided consistent results in measuring global and regional MBF values, suggesting that they may be used interchangeably to process data acquired with a common imaging protocol. (J Am Coll Cardiol Img 2014;■:■–■) © 2014 by the American College of Cardiology Foundation.

From the *Turku PET Centre, University of Turku and Turku University Hospital, Turku, Finland; †IM Sechenov Institute of Evolutionary Physiology and Biochemistry RAS, St. Petersburg, Russia; ‡Lausanne University Hospital, Lausanne, Switzerland; §Regional Cancer Institute of Montpellier (ICM)–Val d'Aurelle, Montpellier, France; ‖University of Florence, Florence, Italy; ¶Siemens Molecular Imaging, Oxford, United Kingdom; #Hokkaido University Graduate School of Medicine, Sapporo, Japan; **Cedars-Sinai Medical Center, Los Angeles, California; ††University of Washington, Seattle, Washington; ‡‡University of Michigan Health Systems, Ann Arbor, Michigan; §§INVIA Medical Imaging Solutions, Ann Arbor, Michigan; ‖‖Department of Nuclear Medicine, Technical University, Munich, Germany; ¶¶Advanced Analytics LLC, Gaithersburg, Maryland; ##National Cardiac PET Center, University of Ottawa Heart Institute, Ottawa, Ontario, Canada; ***University College London, London, United Kingdom; and †††Cardiovascular Imaging Technologies, Kansas City, Missouri. This study was conducted within the Finnish Centre of Excellence in Cardiovascular and Metabolic Diseases supported by the Academy of Finland, University of Turku, Turku University Hospital, and Åbo Akademi University; and was supported in part by grants from the Japanese Ministry of Education, Science and Culture (No. 1959135), Northern Advancement Center for Science & Technology (H23-S2-17),

ABBREVIATIONS AND ACRONYMS

CAD = coronary artery disease

ICC = intraclass correlation coefficient

1TCM = 1-tissue compartment model

LV = left ventricle

MBF = myocardial blood flow

MFR = myocardial flow reserve

RCA = right coronary artery

SP = software package

Measuring myocardial blood flow (MBF) in absolute terms with positron emission tomography (PET) is now possible in clinical routine practice (1). These measurements at rest and under stress can be completed quickly (2,3), and the reconstructed dynamic images can be analyzed in a few minutes by the majority of the available software packages (SPs) (4). The analysis produces left ventricle (LV) absolute MBF values measured in ml/min/g at rest and under stress as well as the myocardial flow reserve (MFR)—the ratio of stress to rest MBF expressed as a unitless number. These values provide unique information regarding diagnosis and monitoring of coronary artery disease (CAD), microvascular health (5), multivessel CAD (6), and risk stratification (7). Although recent studies have shown the diagnostic and prognostic value of MBF quantification over the standard relative image analysis (6,8,9), and use of the generator-produced rubidium-82 (^{82}Rb) (10,11) has brought MBF quantification closer to the clinic, its integration into clinical routine practice remains underutilized (5).

To convert imaging data to quantitative MBF parameters, measured radioactivity concentration values need to be transformed into milliliters of blood per minute per gram of myocardial tissue (ml/min/g) by applying tracer kinetic modeling to dynamic PET images. Thus, any numerical value that any professional receives from ^{82}Rb PET is a result of this transformation. At least 8 different models have been proposed (12–19) for ^{82}Rb. Although deKemp et al. (20) and Tahari et al. (21) had addressed the reproducibility of ^{82}Rb PET analysis methods for MBF quantification, they had focused on a limited number of methods; therefore, a comprehensive comparison study was needed to analyze the current situation in ^{82}Rb PET quantification to help establish common and robust methods to support collaborative multicenter clinical trials.

The objective of the RUBY project was to compare *all* currently available SPs that can analyze ^{82}Rb PET MBF studies. The criteria for inclusion were the presence of the software in the peer-reviewed literature and the willingness of the development team to collaborate according to same ground rules, including blind analysis of the same selected patient datasets. The 10 SPs compared in the present study were: Carimas (22), Corridor4DM (23), FlowQuant (24), HOQUTO (19), ImagenQ (25), MunichHeart (16), PMOD (26), QPET (26), syngo MBF (26), and UW-QPP (18). For further details on the SPs, please see "The Evaluated Software Packages" section in the Online Appendix; for the side-by-side comparison of the packages, see **Table 1** in Saraste et al. (4).

METHODS

IMAGE ACQUISITION. All ^{82}Rb PET studies were performed at the Department of Nuclear Medicine of the University Hospital of Lausanne (Switzerland), according to the routine clinical practice. The study protocol was approved by the local ethics committee. Written informed consent was obtained from each patient prior to the study. Forty-eight patients with suspected or known CAD underwent rest and adenosine-induced stress ^{82}Rb PET. Patients were studied after an overnight fast and were instructed to refrain from caffeine- or theophylline-containing products or medications for 24 h before the ^{82}Rb PET study. During the study, patients were instructed to breathe normally. For further details about the PET image acquisition, please see the Online Appendix.

IMAGE ANALYSIS. The reconstructed rest and stress images were delivered to 10 facilities located in 10 centers across 7 countries. Each investigator used 1 SP and, by the rules of this project, had been blinded to results of the image analysis of the other readers before sharing his or her results (see Online Appendix for details of the study design).

and the U.S. National Institutes of Health grant K25-HL086713. Cedars-Sinai receives royalties from the licensing of QPET software, a minority of which is shared with developers, including Drs. Slomka and Germano. Dr. Slomka has received grant support from Siemens Healthcare. Dr. Alessio has received a research grant from GE Healthcare and has served as a consultant for Lantheus Medical Imaging. Dr. Ficaro has received revenue shares from the sale of Corridor4DM and is the owner of INVIA Medical Imaging Solutions. Dr. Lee has received financial support from and is an employee of INVIA Medical Imaging Solutions. Drs. deKemp and Klein have received revenue shares from the sale of FlowQuant; and have served as consultants to and received revenue shares from Jubilant-DraxImage. Dr. deKemp has received royalties from technologies licensed to Jubilant DraxImage and INVIA Medical Imaging Solutions. Drs. Case and Bateman are owners of Cardiovascular Imaging Technologies, which licenses and sells ImagenQ. Dr. Bateman has served on the advisory board of Lantheus Medical Imaging, GE, and FluoroPharma. Dr. Knuuti has served as a consultant to Lantheus Medical Imaging. All other authors have reported that they have no relationships relevant to the contents of this paper to disclose. Drs. Nesterov and Deshayes contributed equally to this work as first authors. Drs. Prior and Knuuti contributed equally to this work as senior authors.

Manuscript received April 10, 2014; revised manuscript received July 9, 2014, accepted August 6, 2014.

TABLE 1 The 8 Kinetic Models Implemented in 10 Software Packages of RUBY-10

	Retention		One-Tissue Compartment				Two-Tissue Compartment	Axially-Distributed
	Yoshida et al. (13)	Lautamäki et al. (16)	Sitek et al. (17)	Lortie et al. (14)	El Fakhri et al. (15)	Katoh et al. (19)	Herrero et al. (12)	Alessio et al. (18)
Carimas				+				
Corridor4DM			+	+	+			
FlowQuant				+				
HOQUTO						+		
ImagenQ	+			+				
MunichHeart		+						
PMOD				+			+	
QPET				+				
syngo MBF				+				
UW-QPP				+				+

In general, all of the 10 packages implemented variations of a 1-tissue compartment model (1TCM) (27). A total of 7 packages implemented the modification of 1TCM suggested by Lortie et al. (14). An eighth package (ImagenQ-Lortie) also used the Lortie et al. (14) 1TCM; however, it used a shorter 2.5-min dynamic sequence (8×12s, 2×27s) interpolated from the original image data. Additionally, 1 SP—UW-QPP—implemented an axially-distributed blood flow model (18), and another—PMOD—used a 2-tissue-compartment model (12) (**Table 1**). The image analysis process in all packages consisted of image reorientation, segmentation of both LV myocardium and cavity, and tracer kinetic modeling. Several packages enabled automatic reorientation and segmentation; others depended on the operator to influence segmentation of regions where modeling would be done. Please see "The Evaluated Software Packages" section in the Online Appendix for details of the image analysis process.

Image analysis resulted in estimated values for 3 parameters: rest MBF, stress MBF, and MFR on global and regional levels. Global presented the average LV value, and regional presented values for the 3 vascular territories in the regions of coronary arteries: the left anterior descending, left circumflex, and right coronary artery (RCA). The vascular territories were in agreement with the 17-segment American Heart Association standard model (28).

STATISTICAL ANALYSIS. The large number of models compared prohibited the use of standard approaches to measure agreement between 2 methods (29), so a custom linear mixed model for the repeated measures (30) was applied to the dataset. The statistical model output included 2 main agreement metrics—intraclass correlation coefficient (ICC) and difference between the values from the implemented kinetic models—both calculated pairwise. The pairwise agreement between models was considered sufficient if the difference was <20% of the median across all programs and with the corresponding ICC being ≥0.75. The criteria for ICC was based on Khorsand et al. (31), and the difference was greater than the pre-defined 20% standard. We also expressed the values as a percent of corresponding medians to demonstrate the scale of differences.

The paired Student *t* test (Microsoft Excel 2013, Redmond, Washington) was used to evaluate the differences between hemodynamic parameters of patients at rest and at pharmacological stress.

BIPLOT ANALYSIS. To visualize the large number of results of the RUBY-10 comparisons, we developed a custom biplot relating the 2 defined metrics—the differences and the ICC values of compared pairs. In this plot, the x-axis shows pairwise differences between the model values and the y-axis shows corresponding pairwise values of 1 − ICC. In this biplot the origin (x = 0 and y = 0) is the point of identity between the compared values, where there is no difference and the intraclass correlation = 1. Thus, values further from the origin are less in agreement: either showing increasing difference or reduced ICC. The pre-defined criteria of agreement were defined as a rectangular region on the biplot. Thus, this biplot visualizes in an intuitive way our pre-defined criteria of agreement—the pairs inside of these borders were considered to have high pre-defined agreement.

RESULTS

PATIENT CHARACTERISTICS AND HEMODYNAMICS. The study population demographic and hemodynamic characteristics are in **Table 2**. During the pharmacological stress test, heart rate increased ($p < 0.001$), whereas blood pressure showed a mild

TABLE 2 Patient Characteristics (N = 48)

Men	35 (73)
Age, yrs	63.0 ± 12.7 (33–87)
Weight, kg	79.0 ± 15.3 (48–116)
Body mass index, kg/m^2	27.00 ± 4.78 (16.0–41.7)
Symptoms	36 (75)
Angina	28 (58)
Dyspnea	27 (56)
Family history of cardiovascular disease	14 (29)
Known CAD	24 (50)
Previous myocardial infarction	15 (31)
Received procedures	20 (42)
Coronary artery bypass graft surgery	5 (10)
Percutaneous coronary intervention	17 (35)
Hypercholesterolemia	29 (60)
Arterial hypertension	38 (79)
Diabetes mellitus	10 (21)
Currently smoking or ex-smoker	28 (58)
Hemodynamics at rest	
Heart rate, beats/min	76.0 ± 17.0 (49–135)
Systolic blood pressure, mm Hg	136.0 ± 22.3 (94–212)
Diastolic blood pressure, mm Hg	71.0 ± 13.3 (46–110)
Rate pressure product, mm/min	10,400 ± 2,870 (6,000–18,900)
Hemodynamics at pharmacological stress	
Heart rate, beats/min	85.0 ± 15.6* (48–135)
Systolic blood pressure, mm Hg	131.0 ± 21.1† (70–183)
Diastolic blood pressure, mm Hg	68.0 ± 15.1† (30–115)
Rate pressure product, mm/min	11,200 ± 2,870‡ (6,100–21,600)

Values are n (%) or mean ± SD (range). *p < 0.001 vs. rest; †p < 0.05 vs. rest; ‡p < 0.01 vs. rest.
CAD = coronary artery disease.

decrease ($p < 0.05$), resulting in a rate pressure product net increase ($p < 0.01$). All 48 patients—including the 1 with 70/30 mm Hg stress blood pressure—tolerated the stress test well.

ABSOLUTE VALUES OF MBF AT REST AND DURING ADENOSINE STRESS AND MFR. Average MBF and MFR values (Table 3) showed marked variation between models. Differences ($p < 0.0001$) between highest and lowest values for any studied parameter were always greater than a factor of 1.5 times. For rest MBF, the ratios between extreme values were 1.7 globally and ~1.8 regionally; for stress MBF, the ratios ranged from 1.9 globally to ~2.2 regionally; and for MFR, the ratios were 1.5 globally and ranged from 1.9 to 2.3 regionally.

AGREEMENT OF GLOBAL LV MBF MEASUREMENTS. The biplots (Figure 1) demonstrated several consistent patterns. The first pattern was that Lortie et al. (14) implementations (green elements) in 8 SPs tended to concentrate close to the origin. The second pattern was that Katoh et al. (19) implemented in HOQUTO (purple elements) provided results that differed greatly from other models on all studied levels for both MBF and MFR. The third pattern was that Sitek et al. (17) implemented in Corridor4DM (red elements) provided MBF values much higher than the others, both at rest and stress. Note also that Yoshida et al. (13) implemented in ImagenQ (yellow elements) was within the pre-defined difference limits globally at rest (up to 19.8% of the median), but showed higher values for stress (up to 35.0% of the median) and for MFR (up to 24.5%).

AGREEMENT OF REGIONAL LV MBF MEASUREMENTS. Regional values generally showed larger differences: up to 41.5% of the median for RCA. Also, over one-half (60%) of ICC values did not fulfill the pre-defined criteria for agreement. Lautamäki et al. (16) as implemented in MunichHeart (pink elements) was within the pre-defined limits globally for MBF and MFR values and also regionally in the left anterior descending and left circumflex arteries, but had somewhat larger differences in RCA (up to 28.5%), and almost all (97%) of the ICC values did not fulfill the criteria of agreement.

Herrero et al. (12) implemented in PMOD (brown elements) exhibited a pattern similar to the Lautamäki model: all of the global differences were below the pre-defined limit, as well as the regional differences except for the RCA values, which were up to 48.3% of the median, yet again almost all the ICC values (97%) did not fulfill the criteria of agreement.

Differences using El Fakhri et al. (15) as implemented in Corridor4DM (light blue elements) were within the pre-defined limits globally and regionally, with the exception of MFR in the RCA where the difference was 30.0% of the median. ICC values in 38% of comparisons were below pre-defined limits; however, discarding the Yoshida, Lautamäki, and Herrero models, ICC values fulfilled the agreement criteria in 80% of remaining comparisons.

Differences between the Alessio model (18), as implemented in UW-QPP, and the other models were generally within the pre-defined limits, yet occasionally were above: 23.5% of the median at rest and 22.5% at stress on the global level. Differences for MFR were low, yet in RCA, the difference was 25.7% of the median comparing to ImagenQ. Almost all (95%) of the ICC values were >0.75.

AGREEMENT OF LV MBF MEASUREMENTS FOR LORTIE 1TCM. Because the Lortie model (14) was the most commonly applied model in the evaluated SPs, specific biplots for inter-Lortie comparisons were created and are displayed in Figure 2; red elements demonstrate the implementations of the model in UW-QPP (red squares) and ImagenQ (red triangles) that were added later to the RUBY project. Globally,

TABLE 3 Myocardial Blood Flow and MFR Values

	Global			LAD			LCx			RCA		
Software (First Author [Ref. #])	**Rest**	**Stress**	**MFR**	**Rest**	**Stress**	**MFR**	**Rest**	**Stress**	**MFR**	**Rest**	**Stress**	**MFR**
Carimas (Lortie et al. [14])	1.11 ± 0.36	2.38 ± 1.04	2.18 ± 0.82	1.12 ± 0.38	2.31 ± 1.09	2.10 ± 0.87	1.08 ± 0.33	2.30 ± 0.92	2.17 ± 0.75	1.16 ± 0.42	2.86 ± 1.32	2.54 ± 1.07
Corridor4DM (El Fakhri et al. [15])	1.08 ± 0.48	2.40 ± 1.10	**2.42 ± 1.16**	1.13 ± 0.49	2.40 ± 1.07	**2.32 ± 1.05**	1.10 ± 0.48	2.39 ± 1.11	**2.37 ± 1.16**	1.02 ± 0.50	2.46 ± 1.24	**2.74 ± 1.75**
Corridor4DM (Lortie et al. [14])	1.23 ± 0.38	2.58 ± 0.97	2.17 ± 0.78	1.31 ± 0.39	2.57 ± 0.91	2.05 ± 0.71	1.20 ± 0.36	2.45 ± 0.94	2.10 ± 0.75	1.20 ± 0.49	2.82 ± 1.28	2.52 ± 1.23
Corridor4DM (Sitek et al. [17])	**1.69 ± 0.61**	**3.57 ± 1.37**	2.23 ± 0.89	**1.79 ± 0.63**	**3.55 ± 1.28**	2.10 ± 0.80	**1.64 ± 0.59**	**3.41 ± 1.34**	2.20 ± 0.89	**1.63 ± 0.70**	**3.81 ± 1.71**	2.57 ± 1.33
ImagenQ (Lortie et al. [14])	1.22 ± 0.58	2.32 ± 0.99	2.02 ± 0.75	1.23 ± 0.58	2.35+1.04	2.02 ± 0.71	1.23 ± 0.64	2.27 ± 1.00	1.98 ± 0.76	1.19 ± 0.58	2.33 ± 1.00	2.10 ± 0.88
ImagenQ (Yoshida et al. [13])	1.01 ± 0.38	**1.85 ± 0.67**	1.93 ± 0.71	**1.00 ± 0.39**	1.80 ± 0.70	1.90 ± 0.69	1.03 ± 0.43	1.84 ± 0.73	1.89 ± 0.68	1.03 ± 0.37	1.94 ± 0.68	2.01 ± 0.82
FlowQuant (Lortie et al. [14])	1.08 ± 0.38	2.35 ± 1.05	2.29 ± 0.98	1.05 ± 0.39	2.29 ± 1.06	2.29 ± 0.99	1.13 ± 0.42	2.32 ± 1.02	2.29 ± 0.99	1.08 ± 0.39	2.48 ± 1.16	2.39 ± 1.13
HOQUTO (Katoh et al. [19])	1.43 ± 0.49	2.11 ± 0.71	**1.58 ± 0.84**	1.45 ± 0.28	**1.66 ± 0.36**	**1.19 ± 0.44**	1.47 ± 0.32	**1.64 ± 0.35**	**1.18 ± 0.45**	1.48 ± 0.32	**1.67 ± 0.40**	**1.19 ± 0.52**
MunichHeart (Lautamäki et al. [16])	1.13 ± 0.37	2.19 ± 0.89	2.06 ± 0.77	1.16 ± 0.37	2.23 ± 0.91	2.05 ± 0.79	1.12 ± 0.41	2.08 ± 0.93	1.99 ± 0.82	1.11 ± 0.37	2.24 ± 0.87	2.13 ± 0.74
PMOD (Herrero et al. [12])	1.15 ± 0.38	2.22 ± 1.18	1.98 ± 0.85	1.23 ± 0.47	2.34 ± 1.30	1.99 ± 1.01	1.23 ± 0.37	2.51 ± 1.45	2.06 ± 0.96	0.96 ± 0.40	1.79 ± 1.14	2.02 ± 1.18
PMOD (Lortie et al. [14])	1.16 ± 0.35	2.62 ± 1.00	2.29 ± 0.74	1.23 ± 0.38	2.60 ± 1.03	2.17 ± 0.70	1.10 ± 0.33	2.40 ± 0.92	2.23 ± 0.74	1.14 ± 0.38	2.88 ± 1.23	2.60 ± 1.05
QPET (Lortie et al. [[14])	1.14 ± 0.30	2.51 ± 0.84	2.30 ± 0.75	1.20 ± 0.31	2.53 ± 0.87	2.18 ± 0.73	1.13 ± 0.29	2.38 ± 0.82	2.18 ± 0.70	1.06 ± 0.33	2.61 ± 0.92	2.61 ± 1.05
syngo MBF (Lortie et al. [14])	1.22 ± 0.38	2.57 ± 0.95	2.23 ± 0.81	1.27 ± 0.39	2.60 ± 1.01	2.14 ± 0.83	1.17 ± 0.37	2.42 ± 0.91	2.19 ± 0.79	1.19 ± 0.45	2.68 ± 1.00	2.46 ± 1.05
UW-QPP (Alessio et al. [18])	**0.97 ± 0.35**	2.12 ± 0.93	2.25 ± 0.94	1.06 ± 0.41	2.14 ± 0.92	2.11 ± 0.84	**0.93 ± 0.32**	1.96 ± 0.85	2.18 ± 0.92	**0.90 ± 0.35**	2.28 ± 1.17	2.65 ± 1.39
UW-QPP (Lortie et al. [14])	1.20 ± 0.37	2.42 ± 0.89	2.09 ± 0.76	1.30 ± 0.43	2.46 ± 0.87	1.96 ± 0.67	1.14 ± 0.34	2.22 ± 0.81	2.02 ± 0.75	1.10 ± 0.40	2.58 ± 1.13	2.48 ± 1.19
Max/min ratio	1.7	1.9	1.5	1.8	2.1	1.9	1.8	2.1	2.0	1.8	2.3	2.3
Average (all models)	1.19 ± 0.45	2.41 ± 1.04	2.14 ± 0.86	1.23 ± 0.46	2.39 ± 1.06	2.04 ± 0.83	1.18 ± 0.44	2.31 ± 1.03	2.06 ± 0.85	1.15 ± 0.47	2.49 ± 1.22	2.33 ± 1.18
99% CI	1.15-1.23	2.31-2.51	2.05-2.22	1.19-1.28	2.29-2.49	1.96-2.12	1.14-1.22	2.21-2.41	1.98-2.14	1.10-1.19	2.38-2.61	2.22-2.45
Median (all models)	1.11	2.20	2.01	1.16	2.16	1.94	1.11	2.08	1.94	1.06	2.27	2.14
Interquartile range (Q_3-Q_1)	1.44-0.87	3.00-1.67	2.55-1.51	1.48-0.90	2.98-1.61	2.48-1.43	1.44-0.86	2.90-1.57	2.52-1.44	1.43-0.80	3.14-1.62	2.84-1.48

Values are mean ± SD (n = 48) unless otherwise indicated. Average, 99% confidence interval (CI), median values, and interquartile range are calculated for n = 720. Minimum (Min) and maximum (Max) values in each column are in **bold**.

LAD = left anterior descending; LCx = left circumflex; MFR = myocardial flow reserve; RCA = right coronary artery.

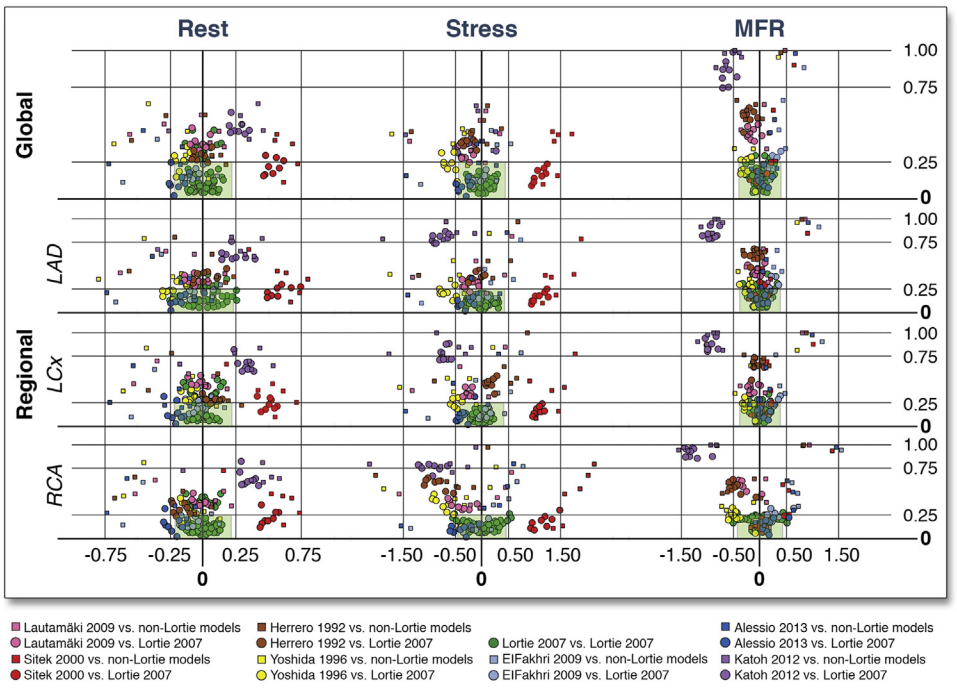

FIGURE 1 Cross-Comparison of Results From All Implemented Models in 10 Software Tools

The x-axis for rest and stress is the difference in myocardial blood flow values (ml/min/g), and for myocardial flow reserve (MFR) is unitless ratios; the y-axis is always 1 − intraclass correlation coefficient. The x-range of the **shaded green area** represents ±20% of the median value. LAD = left anterior descending; LCx = left circumflex; RCA = right coronary artery.

all of the stress differences were well within the pre-defined limits of agreement, <20% of the median value, and the majority of rest differences were also within this limit (except for the ICC values comparing with ImagenQ-Lortie). Similar patterns were observed regionally: the majority of stress MBF values were well within the pre-defined limits. However, in general, regional differences seemed to be larger in the RCA region. Values of the largest differences between implementations of the 1TCM of Lortie et al. (14) are shown in **Table 4**.

DISCUSSION

RUBY-10 is the first and currently the only study aimed at comparing all existing software tools—used both in clinical cardiology and in the research setting—for analyzing MBF and MFR with the most widely used cardiac PET tracer: ^{82}Rb.

The positive finding of our study is that the 1TCM model described by Lortie et al. (14)—commonly found in most PET analysis programs—provided results generally close enough to be used interchangeably, if dynamic time binning protocols are the same. We must emphasize that without an absolute reference standard—such as microsphere data—we cannot infer the diagnostic or quantitative accuracy of any of the methods considered. Despite this, our results do demonstrate that applying the same kinetic model to the same ^{82}Rb PET data, the received MBF and MFR values are independent of the SP within the specified agreement tolerances.

The negative finding is that different kinetic models currently used in ^{82}Rb PET produce different values for the same PET data. The finding is not new: in 2005, Khorsand et al. (32) found differences comparing 1TCM with 2-tissue-compartment model for ^{13}N-ammonia PET. New is the magnitude of possible differences: in the referred study; global differences were up to 13% for MBF and up to 26% for MFR, and our results demonstrate that for ^{82}Rb PET global differences can be up to 90% for MBF and 50% for MFR. Regional differences can be up to 130% for both MBF and MFR.

The causes of differences can vary. In some cases, smoothing of the data can result in higher MBF (33) for factor-analysis-based methods such as Sitek et al. (17) and El Fakhri et al. (15) in Corridor4DM, and minimal filtering is recommended for improved MBF

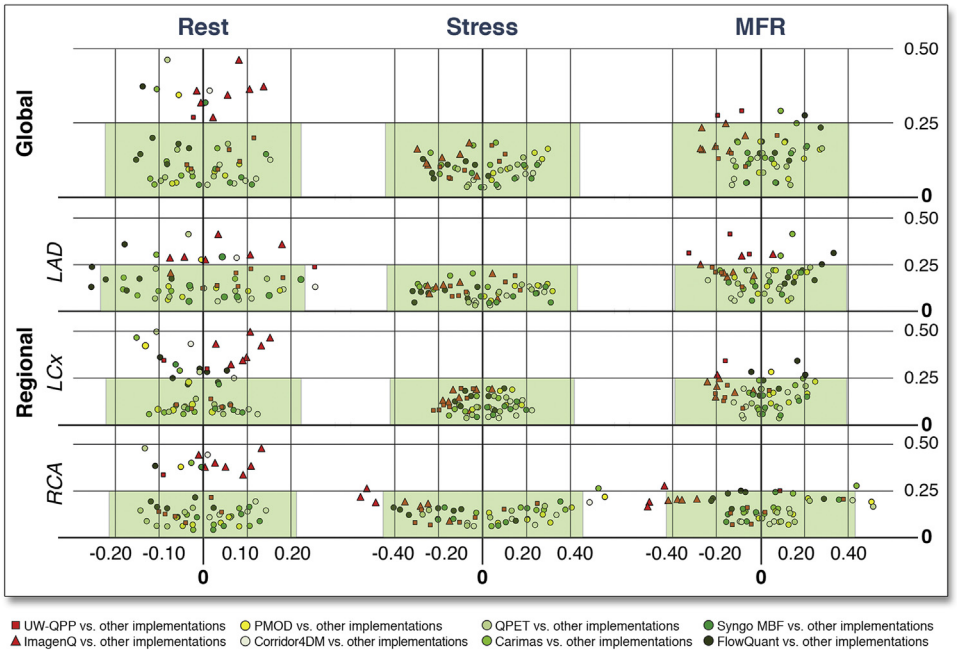

FIGURE 2 **Cross-Comparison of Results From Implemented Lortie Models in 8 Software Tools**

The x-axis for rest and stress is the difference in myocardial blood flow (MBF) values (ml/min/g), and for MFR is unitless ratios; the y-axis is always 1 − intraclass correlation coefficient. The x-range of the **shaded green area** represents ±20% of the median value.

estimates. In others, the difference in prompt-gamma corrections for ^{82}Rb between the PET computed tomography scanner used to perform the current study and the PET studies used originally to develop HOQUTO could be the cause of the difference (34). Notwithstanding the causes, the practical implication is clear: values of MBF or MFR presented without reference to the kinetic model cannot be directly compared, neither for pooling of patient data, nor for following up the same patients.

Two metrics, derived from our statistical model, were used to indicate the agreement—ICC and differences between the compared MBF and MFR values. The benefit of using ICC was clear: it avoids the limitation of standard correlation coefficients—often met in comparison studies—when a linear relationship is mistaken for agreement. However, like other correlation coefficients, ICC depends on the range of variables measured, and this can explain its lower value for rest MBF and MFR compared with stress. The choice of limits of agreement is critical, and for ICC we used recommended (31) values—a cutoff for excellent agreement at over 0.75. For the differences, the choice of appropriate limit is not that straightforward, and we chose to use <20% difference in studied parameters as acceptable, as it is similar to the test-retest repeatability of 20% to 25% for rest MBF and MFR reported recently using ^{82}Rb PET (35).

Increasing the number of compared models geometrically increases the results, which makes the analysis and display of these results challenging. For the measured global and regional values, there were 2,520 differences ($210 \times [3 + 9]$) and 1,260 ICC values; listing all of these values is impractical. The biplot binds these values, and with pre-defined cutoffs informs on the relative agreement of the model results. Therefore, the developed biplots were enabled to handle the complexity of the data inherent in a cross-comparison of this scale.

The analysis of a dynamic PET scan goes through several steps—reorientation, myocardial segmentation, selection of the input function, kinetic modeling, and polar plot generation—each of which could significantly affect the results. We designed our study to simulate the clinical routine practice as much as possible and treated the workflow inside of each SP as a "black box" being only interested in input (the patient PET images) and the output (the results in milliliters [MBF] or ratio units of MFR). As all of the studied SPs were operated either by their developers

TABLE 4 Largest Differences Between Software Packages Implementing Lortie et al. (14)

	Difference (Absolute)*	Difference (Percent of Median)	SW Name	SW Name	p Value	ICC
Global						
Rest	0.15	13.7	C4DM	FQ	0.0008	0.874
Stress	0.30	13.5	PMOD	ImagenQ	0.0019	0.837
MFR	0.28	13.7	QPET	ImagenQ	0.0068	0.835
LAD						
Rest	0.25	22.0†	C4DM	FQ	<0.0001	0.869
Stress	0.32	14.7	PMOD	FQ	0.0020	0.892
MFR	0.33	17.0	FQ	UWQPP	0.0010	0.689
LCx						
Rest	0.15	13.7	ImagenQ	C2	0.0016	0.533
Stress	0.22	10.8	C4DM	UWQPP	0.0356	0.922
MFR	0.25	12.6	PMOD	ImagenQ	0.0134	0.768
RCA						
Rest	0.14	13.5	C4DM	QPET	0.0039	0.854
Stress	0.56	24.5‡	PMOD	ImagenQ	<0.0001	0.782
MFR	0.51	24.0	QPET	ImagenQ	0.0001	0.834

*Differences between MBF values are in units of ml/min/g; differences between MFR are in unitless ratios. †In LAD there are 2 values >20% of the corresponding median, both involving FQ. ‡In RCA (both stress and MFR) there are 3 values >20%; all 3 involve ImagenQ.

MBF = myocardial blood flow; SW = software; other abbreviations as in Table 3.

or under their close supervision, we believe that the tools were used appropriately.

STUDY LIMITATIONS. The most significant limitation of this study is that there was no gold standard used, and thus, no claim of quantitative accuracy of a particular model can be inferred by these results. Another consideration is that the ImagenQ analysis used interpolated dynamic image frames to produce a dataset compatible with this implementation of the Lortie model. The shortened dynamic sequence used by ImagenQ may tend to exaggerate any differences from later uptake and washout frames that were used by the other Lortie models. Last, 1 of the limitations of the study is that 1 software tool, ImagenQ, was added after the preliminary results had been already received. The same approach led to inclusion of the 2 Lortie models: UW-QPP and ImagenQ, which were implemented after receiving preliminary (study average) results of RUBY. These decisions were made for the sake of comprehensiveness, because it would have been practically impossible to repeat the study de novo, so we chose to include these analyses in the primary results. However, these analyses were still performed blinded to the individual results of the other software programs.

We do not consider a limitation the fact that we used only ^{82}Rb data coming from 1 center, acquired on 1 scanner, reconstructed with 1 algorithm, and so on, because introducing these new variables into our combinatorial study would have led to a practical impossibility to carry out the project.

CONCLUSIONS

MBF and MFR values obtained by ^{82}Rb PET must be interpreted together with information on their computational origin. The most important part of such information may not be the software program used to obtain these values, but rather the mathematical tracer kinetic model implemented within the software. The most widely implemented model for ^{82}Rb PET is the 1TCM published by Lortie et al. (14) available in 8 software tools out of the studied 10. When different implementations of this kinetic model are used to analyze the same data, the results appear to be independent of the particular SP utilized. The quantitative blood flow results agree well between these analysis programs and may be used interchangeably for the benefit of large multicenter trials.

ACKNOWLEDGMENTS The authors thank Vesa Oikonen (Turku, Finland) for his everyday advice on kinetic models; Dr. Kim Holmberg (Turku, Finland) for his effort to develop the network analysis method for RUBY-10; Dr. Cyril Burger (Zürich, Switzerland) for his instruction in using PMOD; and Drs. Shana Elman and James Caldwell at the University of Washington (Seattle, Washington) for their expertise in analyzing the data.

REPRINT REQUESTS AND CORRESPONDENCE: Dr. Sergey V. Nesterov, University of Turku and Turku University Hospital, Turku PET Centre, Kiinamyllynkatu 4-8, 20520 Turku, Finland. E-mail: sergey.nesterov@tyks.fi.

REFERENCES

1. Knuuti J, Saraste A. Advances in clinical application of quantitative myocardial perfusion imaging. J Nucl Cardiol 2012;19:643–6.

2. Nakazato R, Berman DS, Dey D, et al. Automated quantitative Rb-82 3D PET/CT myocardial perfusion imaging: normal limits and correlation with invasive coronary angiography. J Nucl Cardiol 2012;19:265–76.

3. Gould KL. Coronary flow reserve and pharmacologic stress perfusion imaging: beginnings and evolution. J Am Coll Cardiol Img 2009;2:664–9.

4. Saraste A, Kajander S, Han C, Nesterov SV, Knuuti J. PET: is myocardial flow quantification a clinical reality? J Nucl Cardiol 2012;19:1044–59.

5. Schindler TH, Schelbert HR, Quercioli A, Dilsizian V. Cardiac PET imaging for the detection and monitoring of coronary artery disease and microvascular health. J Am Coll Cardiol Img 2010;3:623–40.

6. Ziadi MC, Dekemp RA, Williams K, et al. Does quantification of myocardial flow reserve using rubidium-82 positron emission tomography facilitate detection of multivessel coronary artery disease? J Nucl Cardiol 2012;19:670–80.

7. Dorbala S, Di Carli MF, Beanlands RS, et al. Prognostic value of stress myocardial perfusion positron emission tomography: results from a multicenter observational registry. J Am Coll Cardiol 2013;61:176–84.

8. Yoshinaga K, Katoh C, Manabe O, et al. Incremental diagnostic value of regional myocardial blood flow quantification over relative perfusion imaging with generator-produced rubidium-82 PET. Circ J 2011;75:2628–34.

9. Farhad H, Dunet V, Bachelard K, Allenbach G, Kaufmann PA, Prior JO. Added prognostic value of myocardial blood flow quantitation in rubidium-82 positron emission tomography imaging. Eur Heart J Cardiovasc Imaging 2013;14:1203–10.

10. Gould KL. Clinical cardiac PET using generator-produced Rb-82: a review. Cardiovasc Intervent Radiol 1989;12:245–51.

11. Yoshinaga K, Chow BJ, Williams K, et al. What is the prognostic value of myocardial perfusion imaging using rubidium-82 positron emission tomography? J Am Coll Cardiol 2006;48:1029–39.

12. Herrero P, Markham J, Shelton ME, Bergmann SR. Implementation and evaluation of a two-compartment model for quantification of myocardial perfusion with rubidium-82 and positron emission tomography. Circ Res 1992;70:496–507.

13. Yoshida K, Mullani N, Gould KL. Coronary flow and flow reserve by PET simplified for clinical applications using rubidium-82 or nitrogen-13-ammonia. J Nucl Med 1996;37:1701–12.

14. Lortie M, Beanlands RSB, Yoshinaga K, Klein R, Dasilva JN, Dekemp RA. Quantification of myocardial blood flow with 82Rb dynamic PET imaging. Eur J Nucl Med Mol Imaging 2007;34:1765–74.

15. El Fakhri G, Kardan A, Sitek A, et al. Reproducibility and accuracy of quantitative myocardial blood flow assessment with (82)Rb PET: comparison with (13)N-ammonia PET. J Nucl Med 2009;50:1062–71.

16. Lautamäki R1, George RT, Kitagawa K, et al. Rubidium-82 PET-CT for quantitative assessment of myocardial blood flow: validation in a canine model of coronary artery stenosis. Eur J Nucl Med Mol Imaging 2009;36:576–86.

17. Sitek A, Di Bella EV, Gullberg GT. Factor analysis with a priori knowledge—application in dynamic cardiac SPECT. Phys Med Biol 2000;45:2619–38.

18. Alessio AM, Bassingthwaighte JB, Glenny R, Caldwell JH. Validation of an axially distributed model for quantification of myocardial blood flow using ^{13}N-ammonia PET. J Nucl Cardiol 2013;20:64–75.

19. Katoh C, Yoshinaga K, Klein R, et al. Quantification of regional myocardial blood flow estimation with three-dimensional dynamic rubidium-82 PET and modified spillover correction model. J Nucl Cardiol 2012;19:763–74.

20. Dekemp RA, Declerck J, Klein R, et al. Multisoftware reproducibility study of stress and rest myocardial blood flow assessed with 3D dynamic PET/CT and a 1-tissue-compartment model of 82Rb kinetics. J Nucl Med 2013;54:571–7.

21. Tahari AK, Lee A, Rajaram M, et al. Absolute myocardial flow quantification with (82)Rb PET/CT: comparison of different software packages and methods. Eur J Nucl Med Mol Imaging 2014;41:126–35.

22. Nesterov SV, Han C, Mäki M, et al. Myocardial perfusion quantitation with 15O-labelled water PET: high reproducibility of the new cardiac analysis software (Carimas). Eur J Nucl Med Mol Imaging 2009;36:1594–602.

23. Ficaro EP, Lee BC, Kritzman JN, Corbett JR. Corridor4DM: the Michigan method for quantitative nuclear cardiology. J Nucl Cardiol 2007;14:455–65.

24. Klein R, Renaud JM, Ziadi MC, et al. Intra- and inter-operator repeatability of myocardial blood flow and myocardial flow reserve measurements using rubidium-82 pet and a highly automated analysis program. J Nucl Cardiol 2010;17:600–16.

25. Saha K. Automated quantification of rubidium-82 myocardial perfusion images using wavelet based approach [PhD dissertation]. University of Missouri-Columbia, 2007; Columbia, Missouri.

26. Slomka PJ, Alexanderson E, Jácome R, et al. Comparison of clinical tools for measurements of regional stress and rest myocardial blood flow assessed with 13N-ammonia PET/CT. J Nucl Med 2012;53:171–81.

27. Coxson PG, Huesman RH, Borland L. Consequences of using a simplified kinetic model for dynamic PET data. J Nucl Med 1997;38:660–7.

28. Cerqueira MD, Weissman NJ, Dilsizian V, et al. Standardized myocardial segmentation and nomenclature for tomographic imaging of the heart. A statement for healthcare professionals from the Cardiac Imaging Committee of the Council on Clinical Cardiology of the American Heart Association. Circulation 2002;105:539–42.

29. Bland JM, Altman DG. Statistical methods for assessing agreement between two methods of clinical measurement. Lancet 1986;1:307–10.

30. Davis CS. Statistical methods for the analysis of repeated measurements. New York, NY: Springer, 2002.

31. Rosner B. Fundamentals of biostatistics. 7th edition. Boston, MA: Brooks/Cole, Cengage Learning, 2011.

32. Khorsand A, Graf S, Pirich C, et al. Assessment of myocardial perfusion by dynamic N-13 ammonia PET imaging: comparison of 2 tracer kinetic models. J Nucl Cardiol 2005;12:410–7.

33. Lee BC, Moody JB, Sitek A. Effects of filtering on Rb-82 myocardial blood flow estimates. J Nucl Med 2013;54 Suppl:1659.

34. Renaud JM, Mylonas I, McArdle B, et al. Clinical interpretation standards and quality assurance for the multicenter PET/CT trial rubidium-ARMI. J Nucl Med 2014;55:58–64.

35. Efseaff M, Klein R, Ziadi MC, Beanlands RS, Dekemp RA. Short-term repeatability of resting myocardial blood flow measurements using rubidium-82 PET imaging. J Nucl Cardiol 2012;19:997–1006.

KEY WORDS CAD, imaging software, PET, rubidium-82, reproducibility

APPENDIX For a supplemental methods section, please see the online version of this article.